

Ultrafast Humidity Sensing by Anisotropic Deformation of Carbon Nitride Nanoribbons for Real-Time Respiratory Monitoring

*Yuye Zhang,^{†,§} Yongxiu Song,^{‡,§} Hong Yang,[†] Kaiyang Chen,[†] Qing Zhou,[†] Yanqin Lv,[†]
Ensheng Xu,[†] Songqin Liu,[†] Yanfei Shen,[†] Lei Liu^{*,‡} and Yuanjian Zhang^{*,†}*

[†]Jiangsu Engineering Laboratory of Smart Carbon-Rich Materials and Device, Jiangsu Province
Hi-Tech Key Laboratory for Bio-Medical Research, School of Chemistry and Chemical
Engineering, Medical School, Southeast University, Nanjing 211189, China

[‡]Institute for Advanced Materials, School of Material Science and Technology, Jiangsu
University, Zhenjiang 212013, China

KEYWORDS: carbon nitride, anisotropic deformation, water molecules, humidity sensor,
respiratory monitoring

ABSTRACT: Developing humidity sensing materials with fast response and high sensitivity was of great interest for many applications from industrial field to human healthcare. Here, we report a carbon nitride nanoribbons (CNNRs)-based humidity sensor. Thanks to the delicate humidity-responsive anisotropic deformation and well-balanced hydrophilic surfaces/hydrophobic framework with rapid adsorption/desorption of water molecules by CNNRs, this humidity sensor possessed an ultrafast response of ca. 50 ms, high reproducibility and selectivity, and linearity in an almost full humidity range. As an example, this sensor was successfully applied to real-time breathing detection, and the as-obtained breathing graphic waveforms exhibited a higher sensitivity than that by the traditional clinic measurements. This work would pave a new way for ultrafast and sensitive humidity sensing by using anisotropic deformation of CNNRs and introduce a new application scheme of humidity sensors in more user-friendly respiratory monitoring with higher resolution.

Humidity sensor plays a significant role from industrial field to human healthcare, since water molecules are ubiquitous and engaged in many processes.¹⁻⁴ Thus, development of humidity transduction pathway with fast response and high sensitivity has drawn much attention.⁵⁻⁸ For this, substantial efforts have been devoted to explore various water sensitive materials such as metal oxide,^{9, 10} carbon materials,^{7, 8, 11} and polymers,¹²⁻¹⁴ which can convert humidity to different physical or chemical signals. Among them, the swelling induced signal transduction has been regarded as an important way for humidity sensing by using hydrophilic polymers (*e.g.* polyvinyl alcohol and polyacrylic acid)^{14, 15} and two-dimensional materials (*e.g.* $\text{H}_3\text{Sb}_3\text{P}_2\text{O}_{14}$ and $\text{Li}_2\text{Sn}_2\text{S}_5$),^{16, 17} due to simple preparation, excellent nature and low cost. However, such transduction generally needs water molecules penetrate the whole humidity sensitive material, unfortunately leading to a slow response and recovery. Decreasing of the thickness can accelerate the water adsorption and desorption,^{7, 8} but for swelling-based sensing, it would simultaneously weaken the deformation extent, making sensitivity low.

Notably, in nature a non-uniform structure often has a larger anisotropic deformation upon atmosphere fluctuation.¹⁸ For example, bean pods show an evident hydration-triggered twist in seed dispersal because of its gradient structure (Figure S1). By following the same principle,¹⁹⁻²¹ developing of anisotropic nanostructures would be promising to get out such dilemma in swelling-based humidity sensing. Recently, covalent-bonded polymeric carbon nitride (CN, also often denoted as $\text{g-C}_3\text{N}_4$) has drawn much attention for wide applications from photocatalysis to optoelectronic (bio)sensing.²²⁻²⁶ It possesses unique triangle heptazine-based units and 2D stacked structure, whose anisotropic arrangement along the intraplanar and interplanar directions is similar to that of bean pods. In addition, CN has tailorable nanostructures and its edge and basal plane have an opposing surface hydrophilicity, both of which are favorable for rapid

adsorption/desorption of water molecules.²⁷⁻²⁹ These features render CN highly appealing for fast and sensitive humidity sensing, but to our knowledge, few related studies have been explored.

Here, we report a CN nanoribbons (CNNRs)-based humidity sensor via anisotropic deformations (Figure 1a). The few layers characteristics and well-balanced affinity for water molecules between hydrophilic edge and hydrophobic framework of CNNRs made the anisotropic deformation rapid and reversible. After coupling to carbon nanotubes via a strong π - π interaction into a network, such delicate deformation could be converted into an easy-measurable resistance change. The CNNRs-based humidity sensor exhibited an ultrafast response of ca. 50 ms, high reproducibility and selectivity, and linearity almost in the full humidity range. As an example, it was successfully applied to real-time respiratory monitoring with a higher sensitivity even under a simpler setup, compared to traditional clinic pulmonary function testing.

RESULTS AND DISCUSSION

Because the ultrathin sensitive layer is supposed to be favor of rapid sensing of humidity, bulk CN (see synthesis processes in Figure S2)³⁰ was chemically tailored into nanoribbons under alkaline condition according to our previous work.²⁷ Distinct to bulk CN that mostly consisted of particles with several micrometers in size (Figure 1b), CNNRs had a uniform width of tens of nanometers and length of several micrometers, as shown by the TEM image in Figure 1c. The FT-IR spectra and elemental analysis (Figure S3) showed that hydrophilic hydroxyl/amino groups were decorated on the edge, meanwhile the relative hydrophobic heptazine skeleton was retained. Similar to dry bean pods, interestingly the CNNRs had a twisted structure (Figure 1d), which was further confirmed by AFM image. Some periodic fluctuations in the height of the CNNRs (Figure 1e) were observed, for instance, the line profiles of axial periodicity of a single CNNR, indicated

by arrows 1 in Figure 1e, was depicted in Figure 1f. Similarly, the in-situ phase image in Figure S4 also displays alternating stripes of light and dark along the single nanoribbon, indicative of a typical twisted structure. The average thickness of CNNRs was measured to be 3.26 ± 0.30 nm according to the height profile of the AFM image (Figure 1g), which corresponds to a few layers of CN. Therefore, twisted CN nanoribbons with a relative hydrophobic framework and hydrophilic edge surface were successfully prepared.

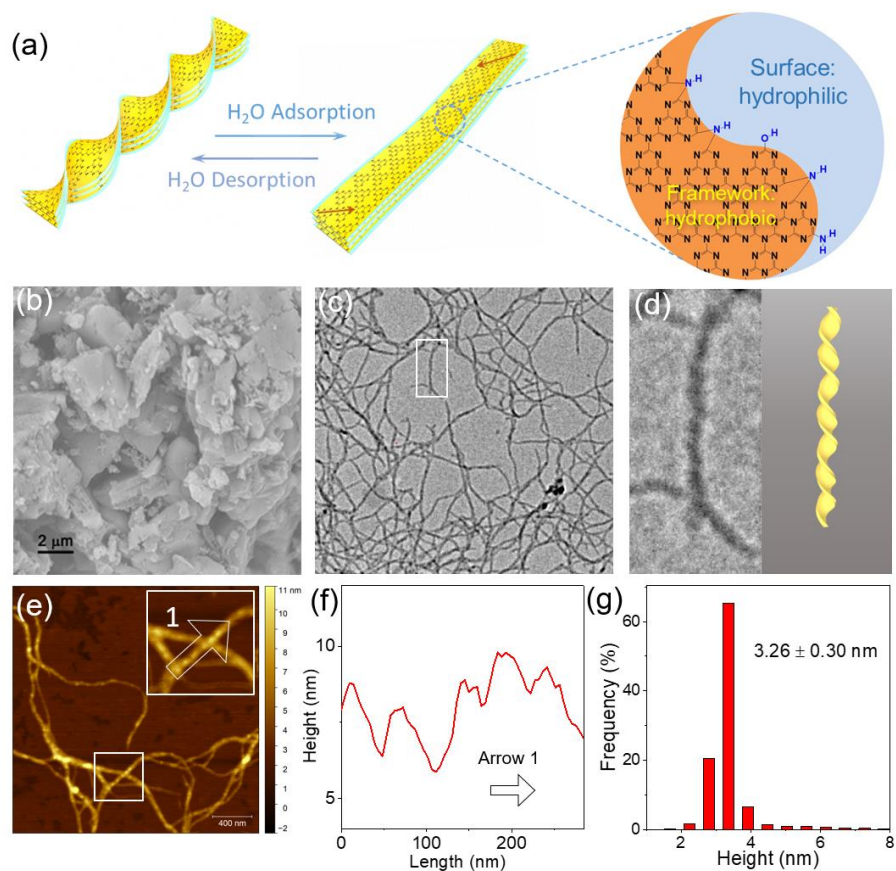


Figure 1. (a) Illustration for deformation of twisted CNNRs and supposed molecular structure of CNNRs. (b) Typical SEM image of bulk CN and (c) TEM image of CNNR. (d) Enlarged TEM image and simulated structure. (e) AFM height image of CNNRs and (f) the line profile of axial periodicity of a single CNNR indicated by arrows 1 in (e). (g) Height distribution of CNNRs.

To demonstrate the deformation of twisted CNNRs upon adsorption/desorption of water molecules, the AFM measurements were carried out at different humidities. The AFM images and the height profiles in Figure 2a-c show that the height of a single CNNR decreased from 3.4 nm to 1.5 nm, and the width of CNNR increased from 62.0 nm to 101.8 nm, namely the height decreased approximately by approximately half, while the width of CNNR nearly doubled, when the environmental relative humidity (RH) increased from 40% to 70%. According to the loss of periodic fluctuation in height (Figure 2d, e), such significant anisotropic swelling could be ascribed to the uncoiling effect via the release of residual stress after absorbing water molecules,^{31, 32} reminiscent of the polymeric nature of carbon nitride that has been rarely explored so far. An evident step in height was also observed for the crossed CNNR in Figure 2e, indicating the softness of rigid CNNR in high humidity. The change in the Young's modulus of CNNRs with different humidity further provided quantitative evidence, which was explored by quantitative nanomechanical mapping.^{33, 34} As shown in Figure 2f, the modulus of CNNRs decreased from 1578 MPa to 48.4 MPa when the humidity increased from 40% to 70%. The adhesion force between the AFM tip and a single CNNR also indicated intrinsic hygroscopicity. As shown in Figure 2g and S5, the maximum adhesion force of CNNR was up to approximately 20.30 nN when the humidity was 70%, while that at the same position was only 8.53 nN when the humidity decreased to 40%. Statistical data for the CNNR (Figure 2h) further confirmed this general trend. It was supposed that the AFM probe was identical in different humidities and had relatively good hydrophilicity, but the Van der Waals interaction between the AFM tip and the sample would be enlarged when the CNNRs absorbed water in high humidity. As control, the adhesion force of the mica surface with good hydrophilicity was maintained almost the same (ca. 20.8 nN) in a humidity of either 40% or 70%. Therefore, the CNNRs were sensitive to humidity, efficiently absorbed

water molecules, and underwent an evident inherent deformation with increasing humidity, making them very promising for humidity sensor construction.

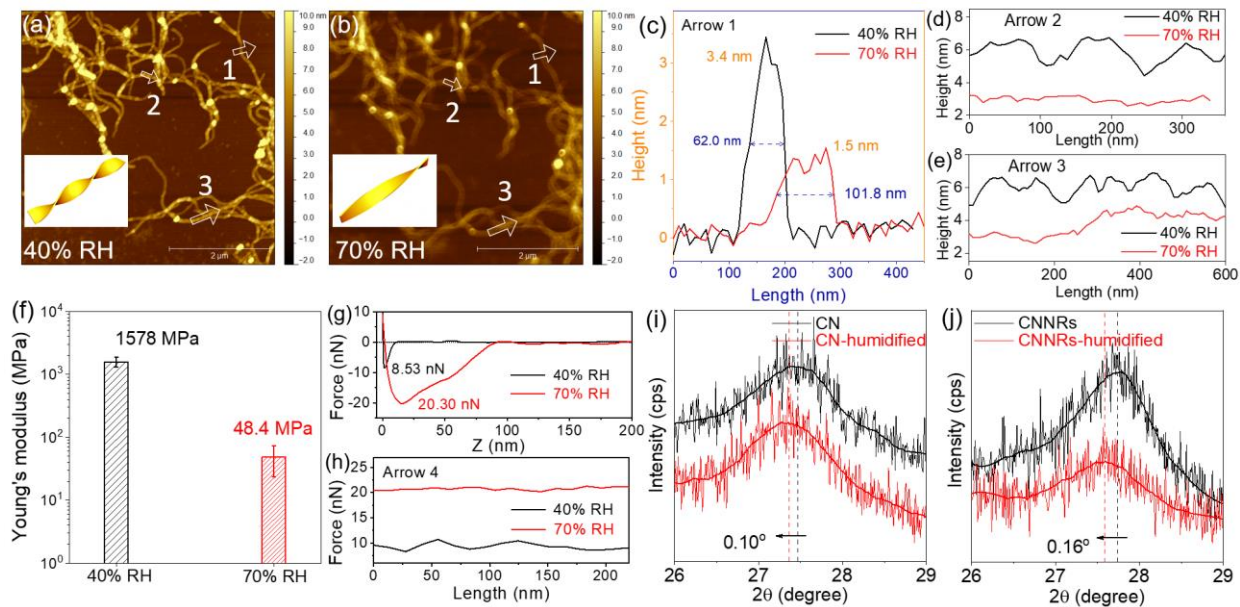


Figure 2. AFM height images of CNNRs in 40% RH (a) and 70% RH (b). Insets: scheme of coiled and uncoiled CNNR. Line profiles of single CNNR indicated by arrows 1 (c), 2 (d) and 3 (e) in (a) and (b). Young's modulus (f), representative adhesion force curve (g) and adhesion line profiles of CNNR (h) indicated by arrow 4 in Figure S5 at different relative humidities of 40% and 70%. XRD patterns of (i) bulk CN and (j) CNNRs before and after humidification, the dashed lines show the (002) diffraction peaks.

To further understanding the interactions between carbon nitride and water molecules, capillary XRD were firstly studied (Figure 2i and j). The interlayer (002) diffraction peak of bulk CN and CNNRs after absorbing water molecules were both found to slightly shift to lower angle, indicative of expanded interlayer distance, but the latter was more evident. It suggested that after tailoring, the absorbing interaction between carbon nitride and water was strengthened and leading to larger swelling, presumably ascribing to the higher density of exposed edges along with more $-NH_x$ and $-OH$ terminals of CNNRs (Figure S3). The hygroscopicity properties of CNNRs was further

studied by contact angle measurement. In general, the NH_x terminals at edges made pristine bulk CN hydrophilic (Figure S6a), but pristine bulk CN demonstrated poor water absorbability, which was supposed to lack of sufficient hydrophilic groups and mostly consist of micro-sized particles. After chemical tailoring, due to the wetted contact by the nanorough surface, a slight increase in the initial contact angle of CNNRs was observed (Figure S6a). Nevertheless, as shown in Figure S6b, the CNNRs exhibited complete absorbing of water droplet in less than 4 s, much faster than the bulk CN (at least more than 30 s), indicating that water absorbability was essentially improved. Moreover, it should be noted that the nanoribbon structure also led to a much higher slit-type porosity ($194.7 \text{ m}^2/\text{g}$) than pristine bulk one ($8.6 \text{ m}^2/\text{g}$, Figure S7). It would be helpful for an efficient transport of water molecules to adsorption sites ($-\text{NH}_x$ and $-\text{OH}$ terminals/defects) throughout the whole CN network and quickly reaching an equilibrium, and vice versa for the desorption processes.

In general, electrical signals are widely used in sensing systems because they can be easily recorded and processed in integrated circuits for application in most electronic devices. Because the conductivity of CN and its derivatives is poor (Figure S8), carbon nanotubes (CNTs) were selected as a reinforcement agent for CNNRs. Although they sense humidity poorly when used alone, CNTs were supposed to boost signal readout, improve water mass transfer and optimize the sensing interface in devices due to their high conductivity, nanostructure (approximately 20 nm in diameter and micrometers in length, Figure S9a, b) and high surface area ($144.3 \text{ m}^2/\text{g}$, Figure S7). Moreover, due to the similarity in conjugated framework, CNTs were ready to be coupled with CNNRs by effective non-covalent π - π interaction (Figure S9c, S9d, and S10). As shown, CNTs could be well dispersed in water by cooperation with the hydrophilic CNNRs by a facile one-step ultrasonic agitation process (Figure S11). Because pristine CNTs were difficult to disperse in

aqueous solution and water is envisioned as the most environmentally friendly solvent for handling, the successful synthesis of homogeneous CNNRs-CNTs in aqueous solution was highly expected for device fabrication and maximization of the unique properties of CNNRs in humidity sensing.

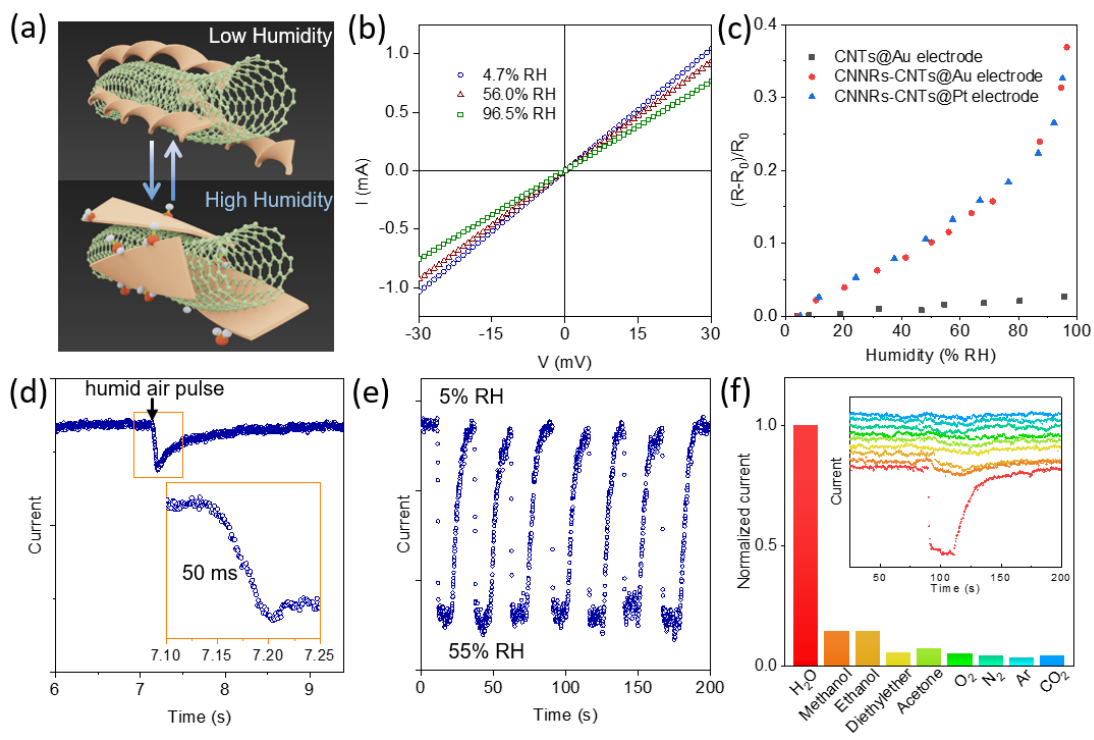


Figure 3. (a) Scheme of CNNRs-CNTs deformation by the absorption/desorption of water molecules. (b) Current-voltage (I - V) curves of CNNRs-CNTs in different relative humidity atmospheres. (c) Relative resistance of CNNRs-CNTs in relative humidity ranging from 5-97%. (d) Response and recovery time under a pulsed flow of humid air. (e) Time-resolved dynamic tests of the sensing signal under different humidities changing between 5% RH to 55% RH for reproducibility test. (f) The normalized current response of the CNNRs-CNTs sensor (inset: I - t curves) in different gases and solvent vapors showing high selectivity.

Because CNNRs deformed in the presence of water vapor, we envisioned that the interconnection of CNTs in the as-prepared CNNRs-CNTs network would be influenced and subsequently,

conductivity would be altered (Figure 3a). Based on this principle, to investigate sensing performance, the CNNRs-CNTs were deposited on an interdigital Au electrode for conductivity measurements via a two-electrode system (see more details in *SI*). Current-voltage (I - V) curves (Figure 3b) were first measured under different relative humidity atmospheres. The linear I - V curves passed through the coordinate origin, in accordance with Ohm's Law and the typical conductor behavior of CNNRs-CNTs. With a gradual increase in the relative humidity, the decreasing of the slope of the I - V curves were observed. It was supposed that upon high humidity the anisotropic deformation of CNNRs occurred, the CNTs were more covered by the low conductive CNNRs, and the interconnection among CNTs would decrease, thus increasing the resistance of the composite (Figure 3a). The sensing signals showed high linearity in a wide range of humidity (Figure 3c), which shows the attractive possibility for realistic humidity sensing. To eliminate the influence of contact resistance between the CNNRs-CNTs network and the substrate, a Pt interdigital electrode was used as a control. Compared with those on the Au electrode, the CNNRs-CNTs on the Pt electrode performed similarly over the entire humidity range (Figure 3c), indicating that the conductivity change originated exclusively from the CNNRs-CNTs rather than from the interface between the CNNRs-CNTs and the metal electrodes.

The development of a humidity sensor with a fast response is highly demanded for real-time respiratory monitoring. The response time in this study is defined as the time for the output signal to reach 90% of the final amplitude.³⁵ The proposed humidity sensor exhibited a response time as low as approximately 50 ms (see the high current to low current, according to the low to high humidity in Figure 3d inset) when humid air was pulsed through dry air. Such a superfast response time was competitive with that of the state-of-the-art humidity sensor (Table S1) .^{5-13, 35-41} Nevertheless, it should be noted that the exact value of response time here does not fully stand for

the real sensing speed in respiratory monitoring, partially because different evaluation methods were used in previous studies. As discussed in the following context, to our knowledge, the resolution of breathing graphic waveforms measured by our CNNRs-CNTs sensor was only challenged by graphene oxide-based system.⁷ The complete recovery time (Figure 3d) reached 1 s, which was supposed to be longer than the real recover time, as the humid air pulse passing through the sensor in the testing pipeline also took a certain of time (see SI for more details). The fast response and recovery times for the CNNRs-CNTs sensor could be ascribed to the following factors: (1) its rapid absorption of water by the nanoribbon structure, (2) the balanced affinity for water molecules from the unique molecular structure of CN, i.e., the opposing hydrophilicity between tri-s-triazine-based 2D framework and $-NH_x$ with $-OH$ terminals/defects in CN (Figure 1a), and (3) the fast mass transfer due to the highly porous structure of CNNRs-CNTs network (Figure S7). The repeatability of the sensor was further tested by changing the ambient humidity between 5% RH and 55% RH. As shown in Figure 3e, the CNNRs-CNTs sensor demonstrated good reproducibility with fluctuating ambient humidity. Therefore, the CNNRs-based humidity sensor had both ultrafast response time and high reproducibility.

Many gases and small organic molecules commonly coexist with water vapor and may significantly interfere with the sensing processes. Interestingly, as shown in Figure 3f, the current did not substantially change after the CNNRs-CNTs sensor was exposed to gases and solvent vapors, such as diethylether, acetone, O_2 , N_2 , Ar, and CO_2 . Moreover, even in the presence of methanol and ethanol, which would form hydrogen bonding with the surface functional groups on CNNRs, only a negligible change in current was observed. This phenomenon may also be ascribed to the small amount of dissolved water in these protic solvents, as water is difficult to remove completely and can easily be enriched from air. In this regard, the CNNRs-CNTs exhibited

excellent overall performance for humidity sensing, i.e., fast response, high reversibility/reproducibility/selectivity/sensitivity, good linearity in almost full humidity range and low cost.

The fast response of the CNNRs-CNTs would enable many applications that require rapid switching in different humidity environments, such as respiratory monitoring (Figure 4a). As shown in Figure 4b, deep and shallow breathing could be easily distinguished by the current-time plot of CNNRs-CNTs sensor. Based on the principle of our methods, a deliberate breath could be recorded using graphic waveforms. As an illustration, a popular Chinese ballad, "ChengDu", was sung by a volunteer three times. The very similar curves with detailed characteristic peaks were obtained (Figure 4c, Movie S1), indicating the feasibility of real-time monitoring of complex breathing processes by the proposed humidity sensor.

In contrast to the above active breathing that is controlled by our brain, eupnea breathing is passively governed by the respiratory centers that receive feedback from the peripheral and central chemoreceptors, and changes under internal and external environments to adapt to requirements for the body metabolism. Thus, the rate, depth and other detailed parameters of eupnea breathing processes are very useful for diagnosing many respiration diseases.^{42, 43} Currently, breathing processes are generally examined using pulmonary function testing stations by means of multiple signals, including nasal/mouth airflow, pressure and volume. Although noninvasive, the sensor needed for these measurements is often in close contact with the body, making patients, especially children, feel anxious and uncomfortable. For example, to obtain precise nasal air flow/pressure, a nasal mask, full-face mask, or cannula is commonly utilized to avoid gas leakage. In this sense, CNNRs-CNTs humidity sensors with ultrafast response as well as excellent selectivity and high

sensitivity can potentially address this problem because water vapor is one of the main constituents of exhaled air and could be measured in an open atmosphere.

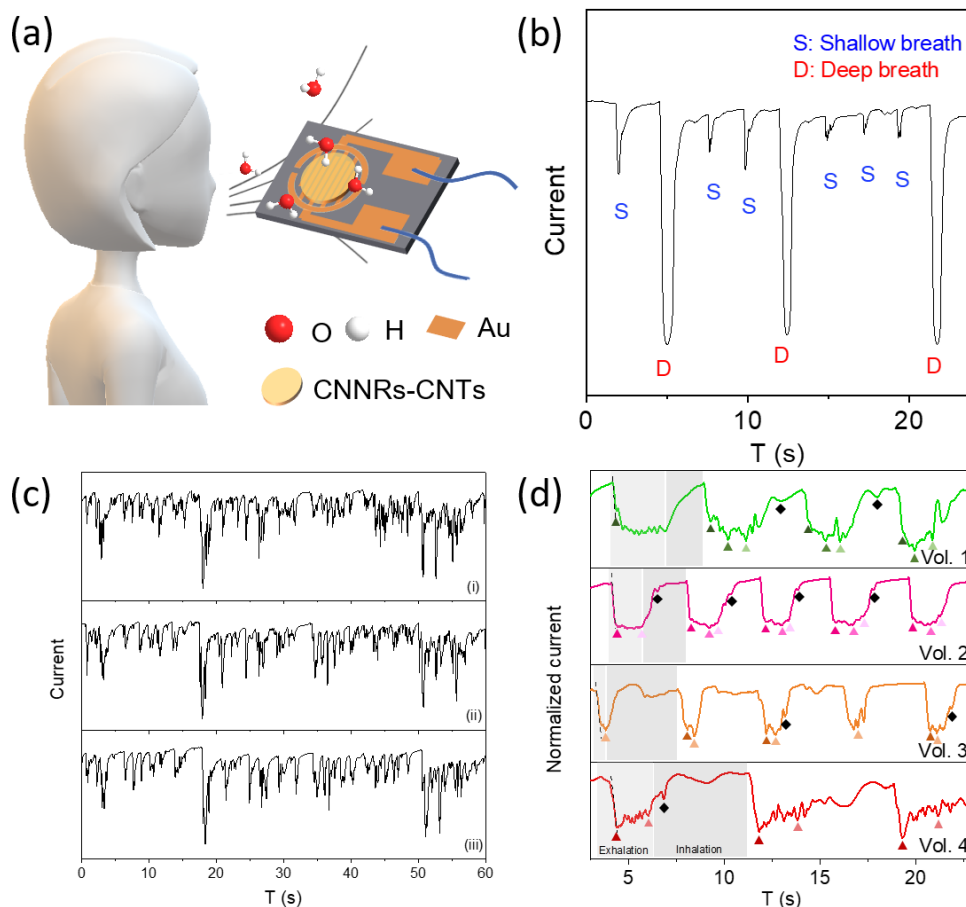


Figure 4. (a) Scheme of breath management using the proposed contactless CNNRs-CNTs humidity sensor in open environment. (b) Current-time plots of human breath for distinguishing deliberate deep breath and shallow breath. (c) Nearly identical breathing graphic waveforms during the recording of the popular Chinese ballad "ChengDu" sung by a volunteer three times (i-iii). (d) Graphic waveforms of breathing in one minute from four selected volunteers (Vol. 1-3: thoracic breathing; Vol. 4: diaphragmatic breathing) detected by the CNNRs-CNTs humidity sensor, showing respiration rate, depth, duration and ratio of ex-/inhalation, maximum airflow rate, stability, and other periodic breathing characteristics (personal features indicated by ▲ in different color sets and general features indicated by ◆).

The performance of the CNNRs-CNTs humidity sensor for contactless noninvasive breath monitoring was examined in real time using the exhaled air from twelve volunteers. From the breathing graphic waveforms, the respiration process of different participants was revealed online in real time (Figure 4d and S12). Fundamental information, such as respiration rate and depth, which represent the basic data of individual physiological indicators, could be easily collected in pace with the fluctuation of exhaled moisture (Table S2). It should be noted that different to humidity sensors in previous pioneering works that mostly revealed respiration rate and depth only,^{7, 35, 37, 44} the CNNRs-CNTs humidity sensor revealed the most comprehensive respiration mechanisms so far to the best of our knowledge, such as duration and ratio of ex-/inhalation (light/dark rectangle highlight), maximum airflow rate (dashed tangent line), and stability (duration of exhalation with constant airflow rate) due to its ultrafast responsivity and high sensitivity (Figure 4d). For instance, the curve for abdominal breathing (Figure 4d, Vol. 4) showed a slower respiration rate and longer ex-/inhalation ratio than that for thoracic breathing (Figure 4d, Vol. 1-3). Moreover, other periodic peaks, assigned to personal breathing characteristics as air was moved into and out of the lungs, were observed for the first times (see the peaks marked by ▲ of different color sets in Figure 4d), suggesting the superior capability of the CNNRs-CNTs to distinguish different types of breathing in the participants. Besides, apart from the individual characteristics, some general features appeared of high probability was also observed in the breathing these volunteers (indicated by ◆ as an example), which may cause by the same muscle movement at the end of exhalation process.

Notably, the sensitivity of the proposed humidity-based CNNRs-CNTs was competitive with or even superior to that of the clinic pulmonary function testing station, as shown by the breathing graphic waveforms based on the traditional air volume measurement (Figure S13). Such graphic waveforms with periodic signals were also reminiscent of the electrocardiogram, suggesting that the as-obtained high-resolution automatic breathing profile may be used as a new diagnostic method for breathing-related diseases with personalized configurations. Different from other respiration-monitoring sensors based on the traditional airflow and pressure measurements, this fast-response CNNRs-CNTs humidity sensor that identifies breathing among individuals would be promising for initiating new applications of humidity sensing in more user-friendly medical equipment and the development of new theories for respiratory mechanisms. For this purpose, further studies are needed to disclose the comprehensive correlation between the breathing humidity-based graphic waveforms and the physical respiration kinetics for clinic disease diagnosis.

CONCLUSIONS

In summary, we report a CNNRs-based humidity sensor with ultrafast response, high reversibility, selectivity, and sensitivity and good linearity in an almost full range of humidity. It was revealed that the delicate humidity-responsive anisotropic deformation and well-balanced affinity for water molecules by CNNRs played the primary roles. As an example, such high-performance humidity sensor was successfully applied to real-time respiratory monitoring in a contactless and open-environment mode, distinct to the sealed manner in traditional clinic airflow and pressure-based measurements, but exhibiting even higher sensitivity. This work provides a new method for

ultrafast and sensitive humidity sensing by using anisotropic deformation of CNNRs and also sheds light on humidity sensing for more user-friendly respiratory monitoring with higher resolution.

MATERIALS AND METHODS

Chemicals and materials. Dicyandiamide (DCDA, 99%) was purchased from Sigma-Aldrich, U.S.A. Sodium hydroxide (NaOH, 96+%) was obtained from Sinopharm Chemical Reagent Co., Ltd., China. Multi-walled carbon nanotubes (CNTs, product number: S-MWNT-1020) was purchased from Shenzhen Nanotech Port Co., Ltd., China. The interdigitated Au and Pt electrodes (product number: ED-IDE3-Au and ED-IDE3-Pt) were obtained from Micrux Technologies, Spain. Ultrapure water (18.2 M Ω cm), obtained from a Smart2Pure 3 purification system (Thermo, U.S.A.), was used in all experiments.

Preparation of CN nanoribbons (CNNRs) and CNNRs-CNTs. CNNRs were prepared according to our previous report. Briefly, the bulk CN was firstly prepared by thermal condensation of DCDA at 550 °C and grinding into fine powders by agate mortar before use. Then, the CN powder (500 mg) was added into NaOH solution (3 M, 20 mL), and the mixture was stirred at 60 °C for 12 h and treated under ultrasonication for 1 h every 4 h. After that, the CNNRs were obtained by removing excessive NaOH via dialysis in a membrane of molecular weight cutoff of 3500 Da (D306-50, Biodesign Inc., U.S.A.) against water until neutral. The CNNRs-CNTs was synthesized by adding CNTs powder (1 mg) to 0.5 mL CNNRs dispersion (8.9 mg/mL), and then the volume of the dispersion was adjusted to be the same (1 mL) using water. The mixtures were ultrasonicated for 15 minutes to obtain the homogeneous CNNRs-CNTs dispersion.

Characterization. Scanning electron microscope (SEM) images were collected on a Zeiss Ultra Plus scanning electron microscopy (Germany). Transmission electron microscope (TEM) images were obtained on a JEM-2100 microscopy (JEOL, Japan). Raman spectra were measured with a DXR-laser micro Raman spectrophotometer ($E_x=532$ nm, Thermo, USA). Elemental analysis (EA) was carried out on a Vario EL Cube analyzer (Elementar, Germany). The XRD patterns were recorded on SmartLab and Ultima IV diffractometers (Rigaku, Japan) in sealed capillaries. The Brunauer–Emmett–Teller (BET) surface area was calculated from 77 K N₂ adsorption-desorption isotherms acquired on Nova 1000e instrument (Quantachrome, USA). All electric measurements were carried on a potentiostat (Gamry Reference 600, USA).

Atomic force microscopy (AFM) measurements. CNNRs solution (10 μ L) were deposited onto the freshly cleaved mica surface and air-dried for 10 min, then the residues were removed. The sample was dried before measurement. The experiments were performed under the ambient conditions (Multimode SPM and Nanoscope V controller, Veeco Instruments). The cantilever (ultra-sharp silicon probe, OMCL-AC160TS-R3, Olympus) had a spring constant of 26 N m⁻¹. For nanoscale material property mapping, the cantilever was calibrated by ramp and thermal tuning beforehand. We imaged samples in Veeco 8 quantitative nanomechanical mapping mode AFM under ambient conditions, which is named peakforce QNM mode with precise force control. Peak-force tapping mode oscillates, but far below the cantilever resonant frequency, the vertical motion of the cantilever using the (main) Z piezo element and relies on peak force for feedback. Peak interaction force and nanoscale material properties were collected for each individual tap. AFM images were performed in tapping mode or peak-force tapping mode at a scan frequency of 1 Hz with optimized feedback parameters and 512 \times 512-pixel resolution. The air humidity of 40% and 70% used for the hygroscopic properties test of CNNRs was controlled by Parkoo dehumidifier

(NO. YDA-870EB, China). The AFM images were collected from up to down at 8 random places and analyzed with NanoScope Analysis software (V1.7) and/or Gwyddion software (V2.51).

Fabrication of CNNRs-CNTs sensor and humidity sensing measurement. Briefly, 5 μL of CNNRs-CNTs dispersion (CNNRs: 0.89 mg/mL, CNTs: 0.2 mg/mL) was deposited on clean Au or Pt interdigitated electrode by drop-casting and naturally drying to obtain CNNRs-CNTs humidity sensor. The static humidity sensing measurement was carried out in a homemade sealed container (25 cm \times 18 cm \times 15 cm). To simulate an environment of different humidity, 200 μL of water was dropped on a 5 cm \times 5 cm cellulose paper in the container. An electric fan was used to force air convection and accelerate volatilization of water to form a moist atmosphere. High purity dry air (99.999%, 79% N₂ and 21% O₂) was used to replace part of the moist air in the container to obtain different humidity. The real-time humidity of the atmosphere was detected by a commercial humidometer (Benetech, China). The I-V plots were performed on the potentiostat. For response-/recovery-time measurement, the CNNRs-CNTs sensor was placed in a silicone pipeline of 8 mm diameter, with a dry air flow passing through (0.1 MPa). To form a humid air pulse, 1 mL of 100% RH air was injected into the up-pipeline (ca. 5 cm) by a syringe. The CNNRs-CNTs sensor responded to the humidity and the signal changed was recorded by the potentiostat. For respiratory monitoring, the CNNRs-CNTs sensor was placed in front of mouths or noses (ca. 5~7 cm away) of volunteers in a non-contact and open environment manner (Movie S1). The CNNRs-CNTs sensor responded to the breathing and the signal changed was recorded by the potentiostat.

ASSOCIATED CONTENT

Supporting Information

The following files are available free of charge: Scheme of anisotropic deformation upon dehydration of bean pod, proposed thermal condensation process of CN, FT-IR analysis, AFM phase image and line profiles of CNNRs, adhesion map of CNNRs in different humidity, contact angles measurement, N₂ adsorption-desorption isotherms, current-Voltage (I-V) plot of CNNRs, SEM and TEM images of CNTs and CNNRs-CNTs, Raman spectra, photograph of CNNRs, CNTs, CNNRs-CNTs aqueous dispersion and scheme of the proposed state of CNNRs-CNTs, comparison of sensors reported in literatures and CNNRs-CNTs sensor, graphic waveforms of human breath from 12 volunteers and summarized breathing kinetics, waveform graphics of volunteer breathing measured by commercial Pulmonary Function Testing system in hospital (PDF)

Video of detecting breathing during the recording of the popular Chinese ballad "ChengDu" sung by a volunteer (AVI)

AUTHOR INFORMATION

Corresponding Author

*E-mail: liul@ujc.edu.cn.

*E-mail: Yuanjian.Zhang@seu.edu.cn.

Author Contributions

§ Y.Y.Z. and Y.X.S. contributed equally to this work.

Y.J.Z. and Y.Y.Z. conceived and designed the experiments. Y.Y.Z. prepared CNNRs, fabricated the sensors and performed the sensing experiments. L.L and Y.X.S. performed the AFM measurements and data analysis. Y.F.S., K.Y.C., Q.Z., Y.Q.L., H.Y., E.S.X., and S.Q.L. contributed to the sensing data collection. All authors contributed to the analysis and discussion of

the results. Y.J.Z., Y.Y.Z., Y.F.S., L.L., and Y.X.S. wrote the manuscript, and all authors reviewed the manuscript. Y.Y.Z. and Y.X.S. had equivalent contributions. Y.J.Z. supervised the project.

Notes

The authors declare no competing financial interest.

ACKNOWLEDGMENT

This work was financially supported in part by the National Natural Science Foundation of China (21775018, 21675022, 21573097), the Natural Science Foundation of Jiangsu Province (BK20160028, BK20170084), the Postgraduate Research & Innovation Program of Jiangsu Province (KYCX17_0137), the Open Funds of the State Key Laboratory of Electroanalytical Chemistry (SKLEAC201703) and the Fundamental Research Funds for the Central Universities. We also thank Prof. X. Zhu and Ms. P. Li in Zhongda Hospital and Prof. J. Cao in Medical School, Southeast University, China for clinical breathing measurements and help discussion.

REFERENCES

- (1) Willett, K. M.; Gillett, N. P.; Jones, P. D.; Thorne, P. W., Attribution of Observed Surface Humidity Changes to Human Influence. *Nature* **2007**, *449*, 710-712.
- (2) Chen, L.; Ye, J. W.; Wang, H. P.; Pan, M.; Yin, S. Y.; Wei, Z. W.; Zhang, L. Y.; Wu, K.; Fan, Y. N.; Su, C. Y., Ultrafast Water Sensing and Thermal Imaging by a Metal-Organic Framework with Switchable Luminescence. *Nat. Commun.* **2017**, *8*, 15985.
- (3) Blank, T. A.; Eksperiandova, L. P.; Belikov, K. N., Recent Trends of Ceramic Humidity Sensors Development: A Review. *Sensor Actuat. B: Chem.* **2016**, *228*, 416-442.

- (4) Trung, T. Q.; Duy, L. T.; Ramasundaram, S.; Lee, N. E., Transparent, Stretchable, and Rapid-Response Humidity Sensor for Body-Attachable Wearable Electronics. *Nano Res.* **2017**, *10*, 2021-2033.
- (5) Squillaci, M. A.; Ferlauto, L.; Zagranyski, Y.; Milita, S.; Mullen, K.; Samori, P., Self-Assembly of an Amphiphilic Pi-Conjugated Dyad into Fibers: Ultrafast and Ultrasensitive Humidity Sensor. *Adv. Mater.* **2015**, *27*, 3170-3174.
- (6) Feng, J.; Peng, L.; Wu, C.; Sun, X.; Hu, S.; Lin, C.; Dai, J.; Yang, J.; Xie, Y., Giant Moisture Responsiveness of Vs2 Ultrathin Nanosheets for Novel Touchless Positioning Interface. *Adv. Mater.* **2012**, *24*, 1969-1974.
- (7) Borini, S.; White, R.; Wei, D.; Astley, M.; Haque, S.; Spigone, E.; Harris, N.; Kivioja, J.; Ryhanen, T., Ultrafast Graphene Oxide Humidity Sensors. *ACS Nano* **2013**, *7*, 11166-11173.
- (8) Yan, H. L.; Guo, S. Y.; Wu, F.; Yu, P.; Liu, H. B.; Li, Y. L.; Mao, L. Q., Carbon Atom Hybridization Matters: Ultrafast Humidity Response of Graphdiyne Oxides. *Angew. Chem. Int. Ed.* **2018**, *57*, 3922-3926.
- (9) Kuang, Q.; Lao, C. S.; Wang, Z. L.; Xie, Z. X.; Zheng, L. S., High-Sensitivity Humidity Sensor Based on a Single SnO₂ Nanowire. *J. Am. Chem. Soc.* **2007**, *129*, 6070-6071.
- (10) Qi, Q.; Zhang, T.; Yu, Q.; Wang, R.; Zeng, Y.; Liu, L.; Yang, H., Properties of Humidity Sensing ZnO Nanorods-Base Sensor Fabricated by Screen-Printing. *Sensor Actuat. B: Chem.* **2008**, *133*, 638-643.
- (11) Han, J. W.; Kim, B.; Li, J.; Meyyappan, M., Carbon Nanotube Based Humidity Sensor on Cellulose Paper. *J. Phys. Chem. C* **2012**, *116*, 22094-22097.

- (12) Xiao, X.; Zhang, Q. J.; He, J. H.; Xu, Q. F.; Li, H.; Li, N. J.; Chen, D. Y.; Lu, J. M., Polysquaraines: Novel Humidity Sensor Materials with Ultra-High Sensitivity and Good Reversibility. *Sensor Actuat. B: Chem.* **2018**, *255*, 1147-1152.
- (13) Vivekananthan, V.; Alluri, N. R.; Purusothaman, Y.; Chandrasekhar, A.; Selvarajan, S.; Kim, S. J., Biocompatible Collagen Nanofibrils: An Approach for Sustainable Energy Harvesting and Battery-Free Humidity Sensor Applications. *ACS Appl. Mater. Inter.* **2018**, *10*, 18650-18656.
- (14) Hwang, S. H.; Kang, D.; Ruoff, R. S.; Shin, H. S.; Park, Y. B., Poly(Vinyl Alcohol) Reinforced and Toughened with Poly(Dopamine)-Treated Graphene Oxide, and Its Use for Humidity Sensing. *ACS Nano* **2014**, *8*, 6739-6747.
- (15) Lee, J.; Cho, D.; Jeong, Y., A Resistive-Type Sensor Based on Flexible Multi-Walled Carbon Nanotubes and Polyacrylic Acid Composite Films. *Solid State Electron.* **2013**, *87*, 80-84.
- (16) Szendrei, K.; Ganter, P.; Sanchez-Sobrado, O.; Eger, R.; Kuhn, A.; Lotsch, B. V., Touchless Optical Finger Motion Tracking Based on 2d Nanosheets with Giant Moisture Responsiveness. *Adv. Mater.* **2015**, *27*, 6341-6348.
- (17) Szendrei-Temesi, K.; Sanchez-Sobrado, O.; Betzler, S. B.; Durner, K. M.; Holzmann, T.; Lotsch, B. V., Lithium Tin Sulfide-a High-Refractive-Index 2d Material for Humidity-Responsive Photonic Crystals. *Adv. Funct. Mater.* **2018**, *28*, 1705740.
- (18) Elbaum, R.; Abraham, Y., Insights into the Microstructures of Hygroscopic Movement in Plant Seed Dispersal. *Plant Sci.* **2014**, *223*, 124-133.
- (19) Ko, H.; Javey, A., Smart Actuators and Adhesives for Reconfigurable Matter. *Accounts. Chem. Res.* **2017**, *50*, 691-702.

- (20) Wang, Z. J.; Zhu, C. N.; Hong, W.; Wu, Z. L.; Zheng, Q., Programmed Planar-to-Helical Shape Transformations of Composite Hydrogels with Bioinspired Layered Fibrous Structures. *J. Mater. Chem. B* **2016**, *4*, 7075-7079.
- (21) Gladman, A. S.; Matsumoto, E. A.; Nuzzo, R. G.; Mahadevan, L.; Lewis, J. A., Biomimetic 4d Printing. *Nat. Mater.* **2016**, *15*, 413-418.
- (22) Lakhi, K. S.; Park, D. H.; Al-Bahily, K.; Cha, W.; Viswanathan, B.; Choy, J. H.; Vinu, A., Mesoporous Carbon Nitrides: Synthesis, Functionalization, and Applications. *Chem. Soc. Rev.* **2017**, *46*, 72-101.
- (23) Volokh, M.; Peng, G.; Barrio, J.; Shalom, M., Carbon Nitride Materials for Water Splitting Photoelectrochemical Cells. *Angew Chem Int Ed Engl* **2019**, *58*, 6138-6151.
- (24) Wang, X.; Maeda, K.; Thomas, A.; Takanabe, K.; Xin, G.; Carlsson, J. M.; Domen, K.; Antonietti, M., A Metal-Free Polymeric Photocatalyst for Hydrogen Production from Water under Visible Light. *Nat. Mater.* **2009**, *8*, 76-80.
- (25) Lau, V. W. H.; Klose, D.; Kasap, H.; Podjaski, F.; Pignie, M. C.; Reisner, E.; Jeschke, G.; Lotsch, B. V., Dark Photocatalysis: Storage of Solar Energy in Carbon Nitride for Time-Delayed Hydrogen Generation. *Angew. Chem. Int. Ed.* **2017**, *56*, 510-514.
- (26) Zhou, Z. X.; Zhang, Y. Y.; Shen, Y. F.; Liu, S. Q.; Zhang, Y. J., Molecular Engineering of Polymeric Carbon Nitride: Advancing Applications from Photocatalysis to Biosensing and More. *Chem. Soc. Rev.* **2018**, *47*, 2298-2321.
- (27) Zhang, Y. Y.; Zhou, Z. X.; Shen, Y. F.; Zhou, Q.; Wang, J. H.; Liu, A. R.; Liu, S. Q.; Zhang, Y. J., Reversible Assembly of Graphitic Carbon Nitride 3d Network for Highly Selective Dyes Absorption and Regeneration. *ACS Nano* **2016**, *10*, 9036-9043.

- (28) Arazoe, H.; Miyajima, D.; Akaike, K.; Araoka, F.; Sato, E.; Hikima, T.; Kawamoto, M.; Aida, T., An Autonomous Actuator Driven by Fluctuations in Ambient Humidity. *Nat. Mater.* **2016**, *15*, 1084-1090.
- (29) Liu, M. J.; Jiang, L., Dialectics of Nature in Materials Science: Binary Cooperative Complementary Materials. *Sci. China Mater.* **2016**, *59*, 239-246.
- (30) Thomas, A.; Fischer, A.; Goettmann, F.; Antonietti, M.; Mueller, J.-O.; Schloegl, R.; Carlsson, J. M., Graphitic Carbon Nitride Materials: Variation of Structure and Morphology and Their Use as Metal-Free Catalysts. *J. Mater. Chem.* **2008**, *18*, 4893-4908.
- (31) Lendlein, A.; Jiang, H. Y.; Junger, O.; Langer, R., Light-Induced Shape-Memory Polymers. *Nature* **2005**, *434*, 879-882.
- (32) Kuang, X.; Roach, D. J.; Wu, J. T.; Hamel, C. M.; Ding, Z.; Wang, T. J.; Dunn, M. L.; Qi, H. J., Advances in 4d Printing: Materials and Applications. *Adv. Funct. Mater.* **2019**, *29*, 1805290.
- (33) Knudsen, J. B.; Liu, L.; Kodal, A. L. B.; Madsen, M.; Li, Q.; Song, J.; Woehrstein, J. B.; Wickham, S. F. J.; Strauss, M. T.; Schueder, F.; Vinther, J.; Krissanaprasit, A.; Gudnason, D.; Smith, A. A. A.; Ogaki, R.; Zelikin, A. N.; Besenbacher, F.; Birkedal, V.; Yin, P.; Shih, W. M.; Jungmann, R.; Dong, M. D.; Gothelf, K. V., Routing of Individual Polymers in Designed Patterns. *Nat. Nanotech.* **2015**, *10*, 892-898.
- (34) Zhang, S.; Andreasen, M.; Nielsen, J. T.; Liu, L.; Nielsen, E. H.; Song, J.; Ji, G.; Sun, F.; Skrydstrup, T.; Besenbacher, F.; Nielsen, N. C.; Otzen, D. E.; Dong, M. D., Coexistence of Ribbon and Helical Fibrils Originating from Hiapp(20-29) Revealed by Quantitative Nanomechanical Atomic Force Microscopy. *Proc. Natl. Acad. Sci. USA* **2013**, *110*, 2798-2803.

- (35) Kano, S.; Kim, K.; Fujii, M., Fast-Response and Flexible Nanocrystal-Based Humidity Sensor for Monitoring Human Respiration and Water Evaporation on Skin. *ACS Sens.* **2017**, *2*, 828-833.
- (36) Nohria, R.; Khillan, R. K.; Su, Y.; Dikshit, R.; Lvov, Y.; Varahramyan, K., Humidity Sensor Based on Ultrathin Polyaniline Film Deposited Using Layer-by-Layer Nano-Assembly. *Sensor Actuat. B: Chem.* **2006**, *114*, 218-222.
- (37) He, J.; Xiao, P.; Shi, J. W.; Liang, Y.; Lu, W.; Chen, Y. S.; Wang, W. Q.; Theato, P.; Kuo, S. W.; Chen, T., High Performance Humidity Fluctuation Sensor for Wearable Devices Via a Bioinspired Atomic-Precise Tunable Graphene-Polymer Heterogeneous Sensing Junction. *Chem. Mater.* **2018**, *30*, 4343-4354.
- (38) Yasaei, P.; Behranginia, A.; Foroozan, T.; Asadi, M.; Kim, K.; Khalili-Araghi, F.; Salehi-Khojin, A., Stable and Selective Humidity Sensing Using Stacked Black Phosphorus Flakes. *ACS Nano* **2015**, *9*, 9898-9905.
- (39) Zhang, Z.; Huang, J.; Yuan, Q.; Dong, B., Intercalated Graphitic Carbon Nitride: A Fascinating Two-Dimensional Nanomaterial for an Ultra-Sensitive Humidity Nanosensor. *Nanoscale* **2014**, *6*, 9250-6.
- (40) Zambov, L. M.; Popov, C.; Abedinov, N.; Plass, M. F.; Kulisch, W.; Gotszalk, T.; Grabiec, P.; Rangelow, I. W.; Kassing, R., Gas-Sensitive Properties of Nitrogen-Rich Carbon Nitride Films. *Adv. Mater.* **2000**, *12*, 656-660.
- (41) Geng, W.; Li, N.; Li, X.; Wang, R.; Tu, J.; Zhang, T., Effect of Polymerization Time on the Humidity Sensing Properties of Polypyrrole. *Sensor Actuat. B: Chem.* **2007**, *125*, 114-119.

(42) Lieske, S. P.; Thoby-Brisson, M.; Telgkamp, P.; Ramirez, J. M., Reconfiguration of the Neural Network Controlling Multiple Breathing Patterns: Eupnea, Sighs and Gasps. *Nat. Neurosci.* **2000**, *3*, 600-607.

(43) American Academy of Sleep Medicine Task Force. Sleep-Related Breathing Disorders in Adults: Recommendations for Syndrome Definition and Measurement Techniques in Clinical Research. *Sleep* **1999**, *22*, 667-689.

(44) Zhen, Z.; Li, Z. C.; Zhao, X. L.; Zhong, Y. J.; Zhang, L.; Chen, Q.; Yang, T. T.; Zhu, H. W., Formation of Uniform Water Microdroplets on Wrinkled Graphene for Ultrafast Humidity Sensing. *Small* **2018**, *14*, 1703848.

SYNOPSIS

